*Inorg. Chem.* **2002**, *41*, 5133–5140


# Synthesis, Structure, and Magnetic Properties of the Single-Molecule Magnet $[Ni_{21}(cit)_{12}(OH)_{10}(H_2O)_{10}]^{16-}$

**Stefan T. Ochsenbein,[1a] Mark Murrie,[1a] Eduard Rusanov,[1b] Helen Stoeckli-Evans,[1b] Chihiro Sekine,[†,1c] and Hans U. Güdel*[,1a]**

*Departement für Chemie und Biochemie, Universität Bern, Freiestrasse 3, CH-3000 Bern 9, Switzerland, Institut de Chimie, Université de Neuchâtel, Avenue de Bellevaux 51, CH-2000 Neuchâtel, Switzerland, and Centre des Recherches sur les Très Basses Temperatures (CRTBT)—CNRS, 25 Avenue des martyrs BP166, F-38042 Grenoble cedex 9, France*

Received April 2, 2002

The preparation of two new compounds containing the cluster $[Ni_{21}(cit)_{12}(OH)_{10}(H_2O)_{10}]^{16-}$ is presented, together with a detailed magnetic investigation of one of the compounds. We found that this cluster shows an unexpected stability and that it exists as different stereoisomers. Compound **1** contains the achiral cluster with a $\Delta-\Lambda$ configuration, and compound **2** contains a pair of enantiomeric clusters with the configurations $\Delta-\Delta$ and $\Lambda-\Lambda$, respectively. Magnetic measurements of **1** in the millikelvin range were necessary to determine the spin ground state of $S = 3$, and they also revealed a magnetic anisotropy within the ground state. A frequency-dependent out-of-phase signal was found in alternating current susceptibility measurements at very low temperatures, which indicates a slow relaxation of the magnetization. Thus, individual molecules are acting as single magnetic units, which is a rare phenomenon for nickel clusters. The energy barrier exhibited by compound **1** has been calculated to be 2.9 K.

## 1. Introduction

Since the discovery of magnetic bistability in dodecamanganese acetate,[2,3] scientific interest in molecular clusters containing magnetic transition-metal ions has soared. A whole class of dodecanuclear manganese clusters showing single-molecule magnet (SMM) behavior now exists.[4−8] Smaller mixed-valence clusters containing only four manganese ions[9−11] have also been found to be SMMs. Furthermore, iron[12−15] and vanadium[16] clusters that display SMM behavior have been reported. Basic requirements for a molecule to function as an SMM are a large spin ground state ($S$) and a negative axial anisotropy ($D$). For a zero-field-split ground state with spin $S$ and $D < 0$ the levels with $M_S = \pm S$ are lowest in energy, resulting in an energy

* Author to whom correspondence should be addressed. E-mail: hans-ulrich.guedel@iac.unibe.ch.

† Permanent address: Department of Electrical & Electronic Engineering, Muroran Institute of Technology, 27-1 Mizumoto-cho, Muroran 050-8585, Japan.

(1) (a) Universität Bern. (b) Université de Neuchâtel. (c) CRTBT—CNRS.
(2) Sessoli, R.; Tsai, H.-L.; Shake, A. R.; Wang, S.; Vincent, J. B.; Folting, K.; Gatteschi, D.; Christou, G.; Hendrickson, D. N. *J. Am. Chem. Soc.* **1993**, *115*, 1804.
(3) Sessoli, R.; Gatteschi, D.; Caneschi, A.; Novak, M. A. *Nature* **1993**, *365*, 141−143.
(4) Aubin, S. M. J.; Sun, Z.; Pardi, L.; Krzystek, J.; Folting, K.; Brunel, L.-C.; Rheingold, A. L.; Christou, G.; Hendrickson, D. N. *Inorg. Chem.* **1999**, *38*, 5329.
(5) Soler, M.; Chandra, S. K.; Ruiz, D.; Davidson, E. R.; Hendrickson, D. N.; Christou, G. *Chem. Commun.* **2000**, 2417.
(6) Soler, M.; Artus, P.; Folting, K.; Huffman, J. C.; Hendrickson, D. N.; Christou, G. *Inorg. Chem.* **2001**, *40*, 4604.
(7) Boskovic, C.; Brechin, E. K.; Streib, W. E.; Folting, K.; Hendrickson, D. N.; Christou, G. *Chem. Commun.* **2001**, 467.
(8) Artus, P.; Boskovic, C.; Yoo, J.; Streib, W. E.; Brunel, L.-C.; Hendrickson, D. N.; Christou, G. *Inorg. Chem.* **2001**, *40*, 4199.
(9) Wang, S.; Tsai, H.-L.; Libby, E.; Folting, K.; Streib, W. E.; Hendrickson, D. N.; Christou, G. *Inorg. Chem.* **1996**, *35*, 7578.
(10) Andres, H. P.; Basler, R.; Güdel, H. U.; Aromi, G.; Christou, G.; Büttner, H.; Rufflé, B. *J. Am. Chem. Soc.* **2000**, *122*, 12469.
(11) Yae, J.; Brechin, E. K.; Yamaguchi, A.; Nakano, M.; Huffman, J. C.; Maniero, A. L.; Brunel, L.-C.; Awaga, K.; Ishimoto, H.; Christou, G.; Hendrickson, D. N. *Inorg. Chem.* **2000**, *39*, 3615.
(12) Barra, A.-L.; Debrunner, P.; Gatteschi, D.; Schulz, C. E.; Sessoli, R. *Europhys. Lett.* **1996**, *35*, 133.
(13) Barra, A.-L.; Caneschi, A.; Cornia, A.; Fabrizi de Biani, F.; Gatteschi, D.; Sangregorio, C.; Sessoli, R.; Sorace, L. *J. Am. Chem. Soc.* **1999**, *121*, 5302.
(14) Goodwin, J. C.; Sessoli, R.; Gatteschi, D.; Wernsdorfer, W.; Powell, A. K.; Heath, S. L. *J. Chem. Soc., Dalton Trans.* **2000**, 1835.
(15) Benelli, C.; Cano, J.; Journaux, Y.; Sessoli, R.; Solan, G. A.; Winpenny, R. E. P. *Inorg. Chem.* **2001**, *40*, 188.
(16) Castro, S. L.; Sun, Z.; Grant, C. M.; Bollinger, J. C.; Hendrickson, D. N.; Christou, G. *J. Am. Chem. Soc.* **1998**, *120*, 2365.

10.1021/ic020252w CCC: $22.00 
Published on Web 08/31/2002

barrier which must be overcome to reverse the direction of magnetization. Ferromagnetically coupled $Ni^{2+}$ clusters are known,[17−19] some with large spin ground states. In addition, the combined effects of a low-symmetry ligand field and spin−orbit coupling can lead to an appreciable zero-field splitting (ZFS) for $Ni^{2+}$.[20−22] Therefore, it should be possible to observe SMM behavior in $Ni^{2+}$ clusters. However, the first reported example of a $Ni^{2+}$ SMM has only recently appeared.[23]

An octanuclear nickel cluster was reported using the ligand citrate ($C(O^-)(CO_2^-)(CH_2CO_2^-)_2$, $cit^{4-}$) in 1977,[24] and seemed to be a good starting point for our efforts in making $Ni^{2+}$ spin clusters. We recently reported the synthesis of two new nickel(2+) citrate clusters, consisting of either twenty-one or seven nickel ions.[25] The crystallization of these clusters was controlled by adjusting the ratio of the solvent and precipitant. However, the formation and crystallization of such species is governed by a number of variables such as metal-to-ligand ratio, temperature, pH, counterions, and solvent. In the hope of understanding the conditions, which favor the formation of large species such as the $Ni_{21}$ cluster,[25] we have started to investigate these parameters. This study has led to the isolation of two new compounds, which contain $Ni_{21}$ clusters similar to that reported by us, thus demonstrating the remarkable stability of this high-nuclearity species. Herein, we report magnetic properties, a determination of the spin ground state, magnetic anisotropy and single-molecule magnet behavior at very low temperature.

## 2. Experimental Section

All reagents were obtained from commercial suppliers and used as received, and all syntheses were carried out under aerobic conditions.

**2.1. $Na_2(NMe_4)_{14}[Ni_{21}(cit)_{12}(OH)_{10}(H_2O)_{10}]$ (1).** A 5.456 g (20.8 mmol) sample of $NiSO_4 \cdot 6H_2O$ was dissolved in distilled $H_2O$ (12.5 mL). To this solution was added 1.748 g (43.7 mmol) of NaOH in $H_2O$ (7.5 mL) to precipitate $Ni(OH)_2$, which was filtered, washed with $H_2O$ (3 × 50 mL), and added to an aqueous solution (10 mL) of citric acid monohydrate (3.642 g (17.3 mmol)). Addition of 5.780 g (31.9 mmol) of $NMe_4OH \cdot 5H_2O$ resulted in a dark green solution of pH 9.24. The solution was reduced to a volume of 18 mL by heating. Aliquots of the concentrated nickel citrate solution were placed in small tubes and mixed with ethanol (0.4 mL solution and either 1.1 or 1.2 mL of EtOH). The tubes were sealed, and green blocklike crystals formed after around four weeks. Anal. Calcd (Found) for $C_{128}H_{348}N_{14}Na_2Ni_{21}O_{155}$ (**1**·$51H_2O$): C, 26.31 (25.76); H, 6.00 (6.04); N, 3.36 (3.24). Selected IR data ($cm^{-1}$): 1597 (br), 1488 (s), 1404 (s), 1298 (m), 1261 (m), 1083 (m), 957 (s), 949 (s), 914 (m), 852 (m), 704 (s).

**2.2. $(NMe_4)_{16}[Ni_{21}(cit)_{12}(OH)_{10}(H_2O)_{10}]$ (2).** The procedure for the synthesis of **2** was the same as for **1**, but different amounts of the reagents were used: 5.457 g (20.8 mmol) of $NiSO_4 \cdot 6H_2O$ was used together with 1.890 g (47.3 mmol) of NaOH, 4.371 g (20.8 mmol) of $H_4cit \cdot H_2O$, and 7.031 g (38.8 mmol) of $NMe_4OH \cdot 5H_2O$. For the crystallization 0.4 mL portions of the concentrated solution were mixed with 1.0, 1.1, or 1.2 mL portions of ethanol. Crystals formed after one week. Anal. Calcd (Found) for $C_{136}H_{404}N_{16}Ni_{21}O_{171}$ (**2**·$67H_2O$): C, 26.21 (25.74); H, 6.53 (6.42); N, 3.60 (3.21). Selected IR data ($cm^{-1}$): 1592 (s), 1488 (s), 1404 (s), 1298 (m), 1261 (m), 1084 (m), 957 (s), 948 (s), 913 (m), 852 (m), 702 (s).

**2.3. $Na_8(NMe_4)_8[Ni_{21}(cit)_{12}(OH)_{10}(H_2O)_{10}]$ (3) and $Na_5(NMe_4)_5[Ni_7(cit)_6(H_2O)_2]$ (4).**[25] Addition of an aqueous solution (15 mL) of NaOH (3.520 g, 88.0 mmol) to an aqueous solution (25 mL) of $NiSO_4 \cdot 6H_2O$ (10.907 g, 41.5 mmol) gave a pale green precipitate, which was collected by filtration and washed with distilled water (3 × 100 mL). Dissolution of this solid in an aqueous solution (20 mL) of citric acid monohydrate (7.985 g, 38.0 mmol) gave a solution of pH 2.94. The pH was raised to 9.20 using $NMe_4OH \cdot 5H_2O$ (12.50 g, 69.0 mmol) and the aqueous solution concentrated to a volume of 35 mL. Aliquots of this solution were taken, mixed with EtOH, and kept in sealed sample tubes (the volumes of EtOH given below permit isolation of pure samples of either **3** or **4**). After one month, tabular crystals of **3** could be isolated from solutions of composition aqueous solution (0.4 mL) and EtOH (either 0.7 or 0.8 mL). The crystals were dried under vacuum. Anal. Calcd (Found) for $C_{108}H_{250}N_8Na_8Ni_{21}O_{138}$: C 24.54 (24.43) H 4.77 (4.83) N 2.12 (2.24). After one week, well-formed rodlike crystals of **4** could be isolated from solutions of composition aqueous solution (0.4 mL) and EtOH (0.9, 1.0, or 1.1 mL). The crystals were dried under vacuum. Anal. Calcd (Found) for $C_{56}H_{148}N_5Na_5Ni_7O_{74}$: C 25.85 (25.84) H 5.73 (5.54) N 2.69 (2.65).

**2.4. X-ray Crystallography.** The intensity data of **1** and **2** were collected at 153 K on a Stoe image plate diffraction system[26] using Mo Kα graphite-monochromated radiation: image plate distance 70 mm, $\phi$ oscillation scans 0−200°, step $\Delta\phi = 1.0°$, $2\theta$ range 3.27−52.1°, $d_{max}-d_{min} = 12.45-0.81$ Å.

Structures **1** and **2** were solved by Direct methods using the program SHELXS-97.[27] The refinement and all further calculations were carried out using SHELXL-97.[28] For **1** the ligand and some of the tetramethylammonium cation H atoms could be included in calculated positions and treated as riding atoms using SHELXL default parameters. It was not possible to include the cluster water H atoms or those of the OH groups, nor was it possible to locate the remainder of the solvent of crystallization H atoms. The non-H atoms were refined anisotropically, using weighted full-matrix least-squares on $F^2$. Only the complex was refined in the final cycles of full-matrix least-squares refinement, the rest of the structure being held fixed. In the unit cell it was possible to locate 2 sodium cations, 14 tetramethylammonium cations disordered over a number of sites, and 41 water molecules. The SQUEEZE routine in PLATON[29] was


(17) Benelli, C.; Blake, A. J.; Brechin, E. K.; Coles, S. J.; Graham, A.; Harris, S. G.; Meier, S.; Parkin, A.; Parsons, S.; Seddon, A. M.; Winpenny, R. E. P. *Chem.—Eur. J.* **2000**, *6*, 2.

(18) Blake, A. J.; Grant, C. M.; Parsons, S.; Rawson, J. M.; Winpenny, R. E. P. *Chem. Commun.* **1994**, 2363.

(19) Serna, Z. E.; Lezama, L.; Urtiaga, M. K.; Arriortua, M. I.; Barandika, M. G.; Cortés, R.; Rojo, T. *Angew. Chem.* **2000**, *112*, 352.

(20) Kahn, O. *Molecular Magnetism*; VCH Publishers, Inc.: New York, 1993; p 15.

(21) El Fallah, M. S.; Rentschler, E.; Caneschi, A.; Sessoli, R.; Gatteschi, D. *Inorg. Chem.* **1996**, *35*, 3723.

(22) Waldmann, O.; Hassmann, J.; Müller, P.; Volkmer, D.; Schubert, U. S.; Lehn, J.-M. *Phys. Rev. B* **1998**, *58*, 3277.

(23) Cadiou, C.; Murrie, M.; Paulsen, C.; Villar, V.; Wernsdorfer, W.; Winpenny, R. E. P. *Chem. Commun.* **2001**, *2666*.

(24) Strouse, J.; Layten, S. W.; Strouse, C. E. *J. Am. Chem. Soc.* **1977**, *99*, 562.

(25) Murrie, M.; Stoeckli-Evans, H.; Güdel, H. U. *Angew. Chem.* **2001**, *113*, 2011−2014.

(26) Stoe & Cie. *IPDS Software*; Stoe & Cie GmbH: Darmstadt, Germany, 2000.

(27) Sheldrick, G. M. SHELXS-97 Program for Crystal Structure Determination. *Acta Crystallogr.* **1990**, *A46*, 467.

(28) Sheldrick, G. M. *SHELXL-97*; Universität Göttingen: Göttingen, Germany, 1999.

(29) Spek, A. L. PLATON/PLUTON version Jan. 1999. *Acta Crystallogr.* **1990**, *A46*, C-34.

**Table 1.** Crystallographic Data for **1** and **2**

| | **1**·41$H_2O$·5EtOH | **2**·67$H_2O$ |
|---|---|---|
| empirical formula | $C_{138}H_{362}N_{14}Na_2Ni_{21}O_{155}$ | $C_{136}H_{404}N_{16}Ni_{21}O_{171}$ |
| *a*, Å | 16.5469(11) | 54.056(3) |
| *b*, Å | 18.9571(15) | 15.5352(11) |
| *c*, Å | 25.597(2) | 40.9093(19) |
| α, deg | 71.11(1) | 90 |
| *β*, deg | 89.31(1) | 123.72(1) |
| *γ*, deg | 64.93(1) | 90 |
| *V*, Å$^3$ | 6807.3(9) | 28576(3) |
| Z | 1 | 4 |
| fw | 5977.31 | 6233.66 |
| space group | $P\bar{1}$ | *C*2/*c* |
| *T*, K | 153(2) | 153(2) |
| *λ*, Å | 0.71073 | 0.71073 |
| $\rho_{calcd}$, g/cm$^3$ | 1.458 | 1.449 |
| $\mu$, mm$^{-1}$ | 1.518 | 1.451 |
| R1[a] | 0.0714 | 0.0641 |
| wR2 | 0.1363[b] | 0.1816[c] |

[a] $R1 = \sum||F_o| - |F_c||/\sum|F_o|$. Only observed reflections ($I > 2\sigma(I)$) used: 1, 16072 reflections; **2**, 10968 reflections. [b] $wR2 = [\sum(w(F_o^2 - F_c^2)^2)/\sum wF_o^4]^{1/2}$; $w = 1/[\sigma^2(F_o)^2 + (0.0000P)^2]$, where $P = (F_o^2 + 2F_c^2)/3$ All data used (24558 reflections). [c] $wR2 = [\sum(w(F_o^2 - F_c^2)^2)/\sum wF_o^4]^{1/2}$; $w = 1/[\sigma^2(F_o)^2 + (0.0863P)^2]$, where $P = (F_o^2 + 2F_c^2)/3$. All data used (26278 reflections).

used to eliminate the remainder of the disordered solvent, and this could be equated to five molecules of ethanol per molecule of complex. In the final difference Fourier synthesis some residual density was still found near the disordered tetramethylammonium cations.

For the structure of **2** the citric acid H atoms were included in calculated positions and treated as riding atoms using SHELXL default parameters. The non-H atoms were refined anisotropically, using weighted full-matrix least-squares on $F^2$. No sodium cations could be located. Only 12 of the $NMe_4$ groups could be located, 10 fully occupied and 2 occupied at 50%, disordered over 4 positions. It was assumed that the remainder may be present in a highly disordered fashion within the disordered residual density. A total of 67 solvent water molecules were located, the majority of which were disordered. The majority of the H atoms either could not be located or were not included. Crystallographic information for **1** and **2** is given in Table 1.

**2.5. Infrared Spectroscopy.** IR measurements were performed on samples pressed into KBr pellets on a Perkin-Elmer FT-IR spectrometer 1720 X.

**2.6. Magnetic Measurements.** The magnetic susceptibility measurements were performed using a SQUID magnetometer. A Quantum Design MPMS-XL SQUID was used in the temperature range 2−300 K to measure powder samples of **1** and **2** (obtained by crushing single crystals). Alternatively, a large single crystal of **1** was measured using a homemade SQUID magnetometer with a miniature $^3He/^4He$ dilution refrigerator that can operate down to 0.08 K at the CRTBT−CNRS in Grenoble.

## 3. Results

**3.1. Structure.** Compound **1** crystallizes in the triclinic space group $P\bar{1}$. It contains the $[Ni_{21}(cit)_{12}(OH)_{10}(H_2O)_{10}]^{16-}$ cluster with 2 $Na^+$ and 14 $NMe_4^+$ counterions. The cluster is identical to that found in the previously reported phase (**3**),[25] but with a different crystal packing in the lattice. Figure 1 displays the cluster of compound **1** in two different views. It can be described as a central planar core with two wings. The clusters in compound **2** exist as a pair of enantiomers in the same crystal with the space group *C*2/*c*. The clusters

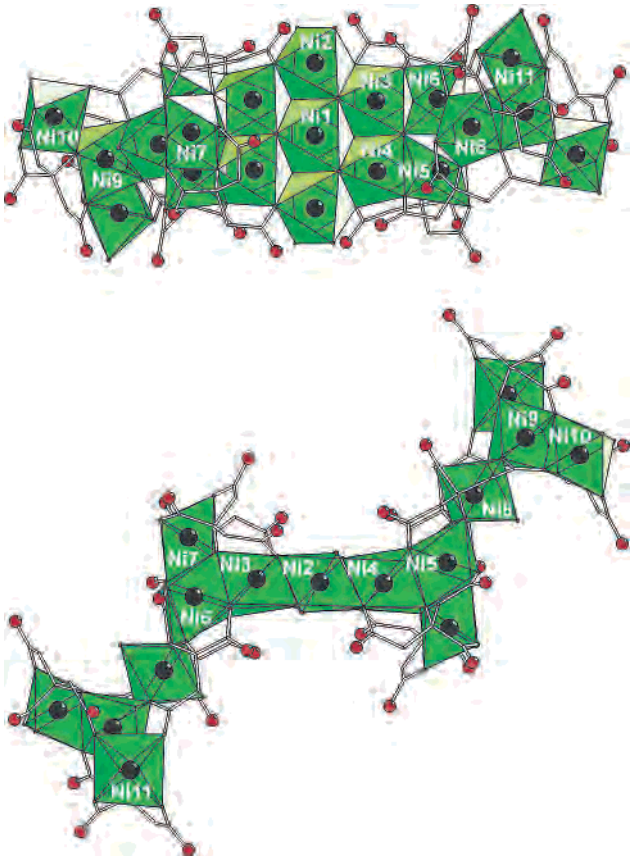


**Figure 1.** Structure of the anion $[Ni_{21}(cit)_{12}(OH)_{10}(H_2O)_{10}]^{16-}$ of **1** in two different views: Ni (black) shown as polyhedra (green), O (red), C (gray), H atoms omitted for clarity.

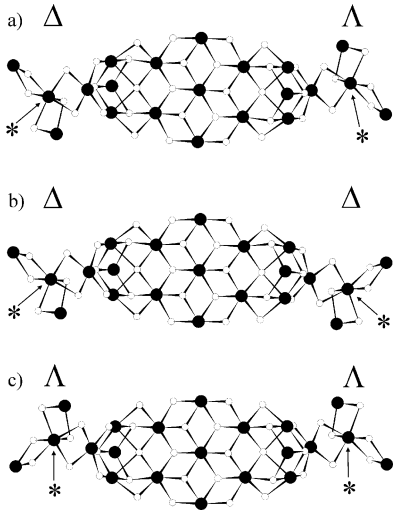


**Figure 2.** Ni−O skeleton (only bridging oxygen atoms shown): (a) Δ−Λ configuration in compounds **1** and **3**, (b) Δ−Δ configuration in **2**, (c) Λ−Λ configuration in **2**. The configurations refer to Ni atoms labeled *.

in **2** are diastereoisomers to the cluster in **1**. The different cluster configurations are depicted in Figure 2. In **1** the clusters form staggered chains along the crystallographic *c*-axis with the two sodium ions located between two clusters. This is shown in Figure 3, which also shows how the cluster lies with respect to the crystallographic axes. The closest intermolecular Ni−Ni distance in **1** is 5.54 Å, whereas in **2** it is longer at 7.77 Å. The connection between the clusters

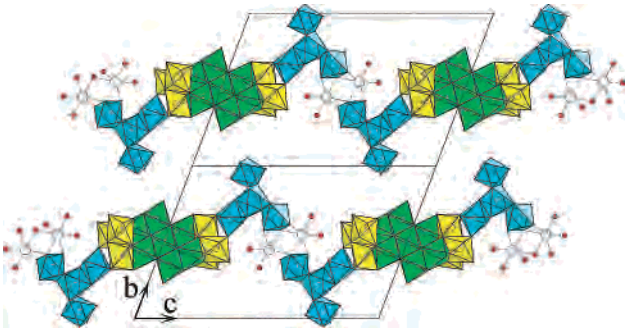


**Figure 3.** Orientation of **1** in the *bc* plane (*b** in the plane, perpendicular to *c*; *a* axis perpendicular to the *bc* plane): Ni−O polyhedra with the $\{Ni_7(OH)_6\}$ core shown in green, core caps in yellow, and wings in blue. Na cations are shown in gray.

in **2** is made by a hydrogen bond of 2.8 Å length between a coordinated water and a citrate oxygen. In **1**, all the clusters are oriented parallel and the central $Ni^{2+}$ ion is located on a center of inversion. A glide plane, where the translational part is along the *c*-axis and the mirror plane is perpendicular to the *b*-axis, relates two enantiomeric clusters in **2**. In addition there is a 2-fold rotation axis through the three central nickel ions.

The core of all these clusters is a $\{Ni_7(\mu_3\text{-}OH)_6\}$ unit, which is a fragment of an extended layer in $Ni(OH)_2$, where the hydroxide ions are hexagonal close-packed and the $Ni^{2+}$ ions occupy the octahedral holes. In the clusters of compound **1** the average Ni−O−Ni bridging angle within the core is 97.53°, with the minimum being 95.44° and the maximum 99.57°, whereas the bridging angles in the core of a cluster of **2** range from 95.20° to 100.15°, yielding an average of 97.29°. Outside the core, the citrate ligand dictates the cluster appearance and the bridging angles display a larger diversity. In clusters of **1** the angles of the Ni−O−Ni alkoxo bridges vary between 79.18° and 127.86°, averaging to 99.30°. The angles of the alkoxo bridges in clusters of compound **2** are similar to the angles in **1** (a complete list of bridging angles is given as Supporting Information).

The citrate ligand was found to exhibit five different binding modes binding three, four, or five nickel ions (see Figure 4). The deprotonated alcohol group provides an alkoxo bridge in all five binding modes. The $\beta$-carboxylates serve as 1,1- and 1,3-bridges, whereas the α-carboxylate serves as a 1,1-bridge in only one of the binding modes. Two additional independent hydroxide ions have been found outside the core bridging either three or four nickel ions. The $\mu_4$-OH shows a distorted square pyramidal coordination geometry to the adjacent nickel ions with trans-bridging angles of 144.08° and 147.31° in clusters of **1** and 145.02° and 146.35° in clusters of **2**. A total of 10 water molecules occupy the remaining coordination sites on the nickel ions, which possess a distorted octahedral coordination.

**3.2. Magnetic Properties.** The magnetic susceptibility of a powder sample (see section 2.6) of **1** measured with an external field of 1 kG is plotted as $\chi T$ versus temperature in Figure 5. It shows a decrease from 26.8 emu $mol^{-1}$ K at 300 K to 20 emu $mol^{-1}$ K at 50 K, where it starts to flatten out before a drop can be observed at about 20 K. The value

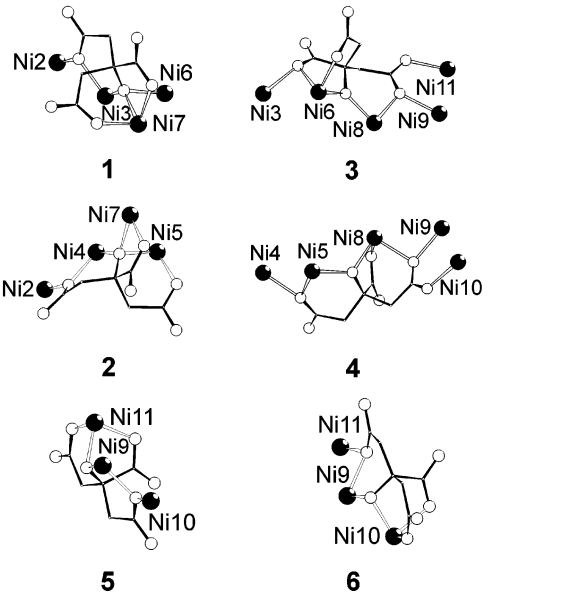


**Figure 4.** The five different binding modes of the citrate ligand found in the $Ni_{21}$ clusters (modes 5 and 6 are equivalent). Ni is represented as a large black sphere, O as a small white sphere, and C as a line, and the H atoms are omitted for clarity.

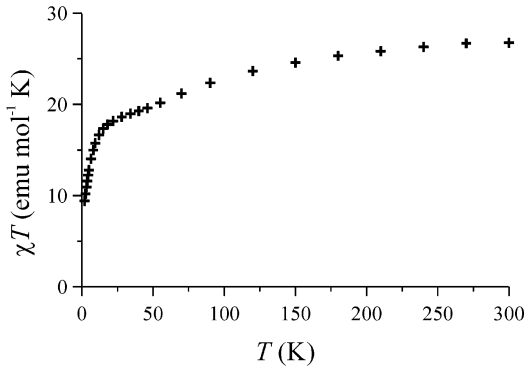


**Figure 5.** A plot of $\chi T$ versus temperature for a powder sample of **1**. The molar magnetic susceptibility $\chi$ was measured in an applied field of 1 kG.

at the lowest observed temperature of 2 K is 9.4 emu $mol^{-1}$ K. The $\chi T$ curves of **1**−**3** were found to be almost identical between 300 and 2 K.

The field dependence of the magnetization for three different orientations of a single crystal of **1** is shown in Figure 6. The measurements were performed at temperatures of 140−180 mK in a field range of 0−7.5 T, along the crystallographic *a*-axis, along the *c*-axis, and perpendicular to the *ac*-plane (we define this direction as the *b**-axis). In the curves obtained with the field parallel to the directions *b** and *c* a clear step appears at approximately 2.5 T, whereas with the field parallel to *a* the step is less pronounced and found at lower field.

On the same crystal, alternating current (ac) susceptibility was recorded down to 100 mK at 11 different frequencies ranging from 0.111 to 1111 Hz. An out-of-phase signal was found for all three orientations of the crystal, with the peak position depending on the frequency, as well as on the orientation of the crystal with respect to the field. Figure 7 displays the temperature dependence of the ac susceptibility for selected frequencies with the field along *b**. The data

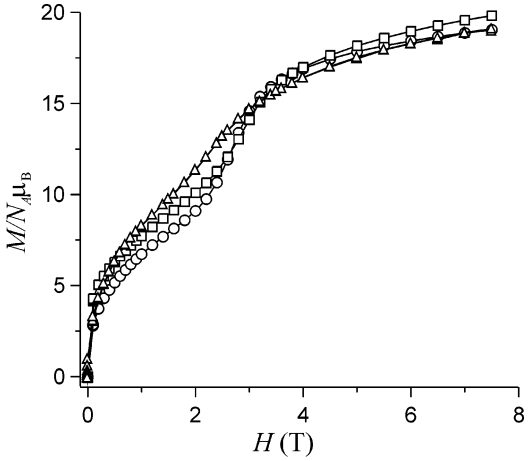


**Figure 6.** Field dependence of the magnetization for three orientations of the crystal of **1**: along *a* at 140 mK (△), along *b** at 140 mK (○), and along *c* at 180 mK (□).

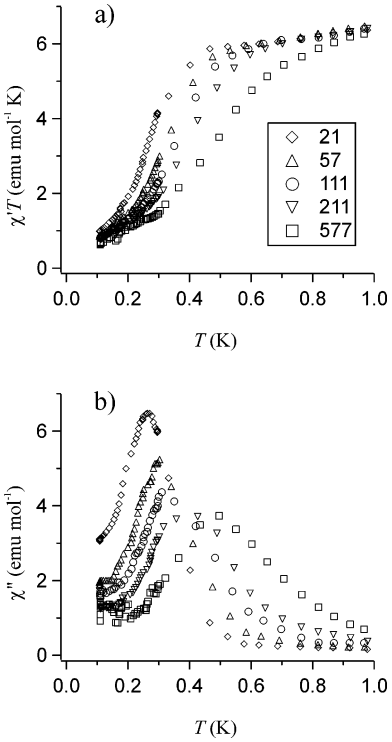


**Figure 7.** A plot of $\chi'T$ vs $T$ (a) and $\chi''$ vs $T$ (b) for a single crystal of **1**. The ac field was applied along *b**, oscillating at the indicated frequencies.

for the ac susceptibility measurements with the field parallel to the crystallographic *c*-axis are shown in Figure 8. The in-phase signals are plotted as $\chi'T$ versus $T$ and the out-of-phase signals as $\chi''$ versus $T$ in both figures. In Table 2 the peak positions obtained by least-squares fitting the out-of-phase peaks with Lorentzian functions are listed for all three orientations of the crystal. The natural logarithm of the relaxation time as a function of the inverse temperature is shown in Figure 9a for the field along *b**. The points lie approximately on a straight line for frequencies between 21 and 1111 Hz, before a flattening of the curve can be observed at lower frequencies. The same kind of plot is shown for the results of the measurements along *c* in Figure 9b. For frequencies between 111 and 1111 Hz the data points are approximately on a straight line prior to a flattening of the curve at lower frequencies.

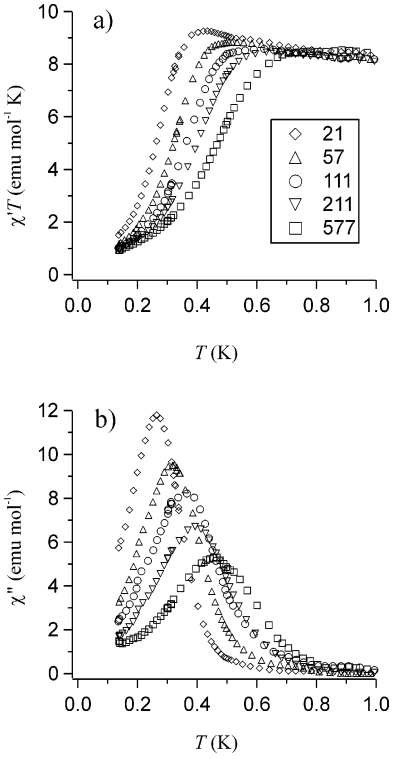


**Figure 8.** A plot of $\chi'T$ vs $T$ (a) and $\chi''$ vs $T$ (b) for a single crystal of **1**. The ac field was applied along *c*, oscillating at the indicated frequencies.

**Table 2.** Out-of-phase ac Susceptibility Results for Three Different Orientations of a Crystal of **1**

| ac freq (Hz) | peak temp (K) | ln(*τ*)[a] | (peak temp (K))$^{-1}$ |
|---|---|---|---|
| | *c* | | |
| 1111 | 0.487 | −8.851 | 2.055 |
| 577 | 0.448 | −8.196 | 2.233 |
| 211 | 0.382 | −7.190 | 2.615 |
| 111.1 | 0.348 | −6.548 | 2.871 |
| 57 | 0.309 | −5.881 | 3.239 |
| 21 | 0.257 | −4.882 | 3.892 |
| 11.1 | 0.223 | −4.245 | 4.485 |
| 2.11 | 0.159 | −2.585 | 6.292 |
| 1.11 | 0.138 | −1.942 | 7.243 |
| | *b** | | |
| 1111 | 0.643 | −8.851 | 1.555 |
| 577 | 0.519 | −8.196 | 1.928 |
| 211 | 0.401 | −7.190 | 2.494 |
| 111.1 | 0.347 | −6.548 | 2.884 |
| 57 | 0.304 | −5.881 | 3.289 |
| 21 | 0.256 | −4.882 | 3.901 |
| 11.1 | 0.225 | −4.245 | 4.441 |
| 2.11 | 0.153 | −2.585 | 6.518 |
| | *a* | | |
| 57 | 0.263 | −5.881 | 3.803 |
| 21 | 0.238 | −4.882 | 4.194 |
| 11.1 | 0.211 | −4.245 | 4.739 |
| 2.11 | 0.152 | −2.585 | 6.590 |
| 1.11 | 0.137 | −1.942 | 7.310 |

[a] The natural logarithm of the relaxation time $\tau$ ($\tau = (2\pi\nu)^{-1}$, with $\nu$ being the frequency of the ac field).

## 4. Discussion

**4.1. Synthesis and Structure.** Compared to the original synthesis, which yielded compounds **3** and **4**,[25] we investi-

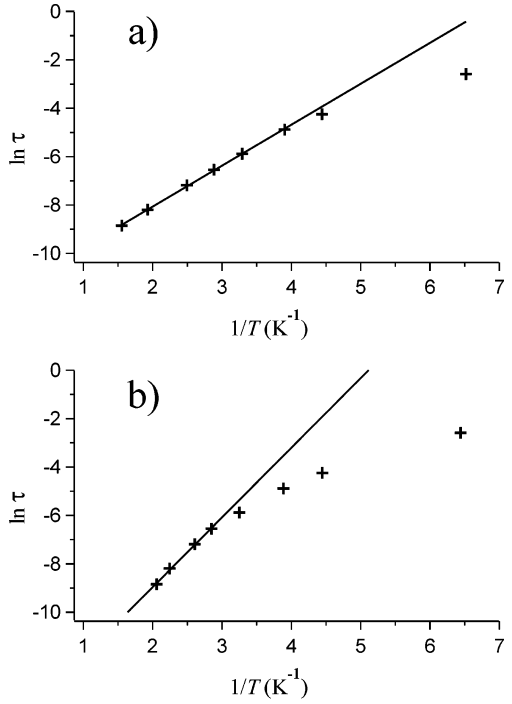


**Figure 9.** ln $\tau$ vs $1/T$ for two orientations of the crystal: along $b^*$ (a) and along $c$ (b). $\tau$ is given by $1/(2\pi\nu)$, with $\nu$ being the frequency at which the field was oscillating. The straight lines are the best fits to an Arrhenius law, eq 3, yielding the parameter values $\tau_0 = 1.1 \times 10^{-5}$ s and $\Delta E = 1.7$ K along $b^*$ and $\tau_0 = 4.0 \times 10^{-7}$ s and $\Delta E = 2.9$ K along $c$.

gated the effect of different $Ni^{2+}$ to citrate ratios and the effect of heat applied during the synthesis. With the different metal to ligand ratios 0.9:1, 1.0:1, and 1.2:1, we obtained the $Ni_{21}$ cluster when heat was applied. The crystallization was carried out under the conditions that yielded **3** and **4**, but the compound containing the $Ni_7$ cluster (**4**) did not crystallize. In the original synthesis (metal:ligand = 1.1:1) the reduction of the solvent was achieved by slow evaporation at room temperature. Therefore, we conclude that the application of heat to the reaction favors the formation of the $Ni_{21}$ cluster over the formation of the $Ni_7$ cluster.

The unexpected stability of this large cluster can be correlated to the presence of the $\{Ni_7(\mu_3\text{-}OH)_6\}$ core, which is the nucleus of the crystallization of $Ni(OH)_2$. The citrate ligand prevents the nucleus from growing and therefore prevents the precipitation of nickel hydroxide. At the final pH of approximately 9.2 the dominant anionic species in solution is $cit^{4-}$, in large excess over $OH^-$. The approximate ratio of $cit^{4-}$ to $OH^-$ is $4 \times 10^4$:1, whereas the ratio $cit^{4-}$:$Hcit^{3-}$ is around 40:1. The p$K_a$ for the fourth deprotonation of citric acid in the presence of $Ni^{2+}$ is approximately 7.6.[30] An indication for the stabilizing effect of the core is the fact that a similar core has been found in cluster chemistry before, namely, in $Fe_{17}$ and $Fe_{19}$ clusters[31] and in portions of a $Co_{24}$ cluster.[32] The presence of a $\mu_4$-OH is rather unusual, but it has been observed before.[33] Moreover, bond valence sum (BVS)[34] calculations endorse this assignment.

As shown in Figure 1, the $Ni_{21}$ anion is built upon a planar edge-sharing $\{Ni_7(OH)_6\}$ core formed by Ni1−Ni4 and symmetry equivalents (se's). If we take half of the molecule, the edge-sharing octahedra Ni5 and Ni6 extend this core by face-sharing with Ni4 and Ni3, respectively. Ni7 shares an edge with both Ni5 and Ni6 and lies above the core plane, completing the compact central body of the cluster comprising 13 $Ni^{2+}$ centers. Ni8 is corner-sharing with Ni5 and Ni6 and shares an edge with Ni9. Completing the wing, Ni9 shares an edge with Ni10 and Ni11. The body−wing arrangement is highlighted in Figure 3, with the planar $\{Ni_7(OH)_6\}$ core shown in green, the core caps completing the body in yellow and the wings in blue. The compact body of the cluster (Ni1−Ni7 and se's, green and yellow octahedra) lies approximately along the $c$-axis.

As shown in Figure 4, the flexibility of ligation exhibited by the ligand citrate is remarkable. In the first mode, the Ni2−Ni3 vector is bridged by a $\mu_2$-$\beta$-carboxylate O donor. The $O^-$ group $\mu_3$-bridges Ni3, Ni6, and Ni7, with the $\alpha$-$CO_2^-$ group and the second $\beta$-$CO_2^-$ group capping Ni7. In mode 2, citrate also bridges four nickel centers. A $\beta$-$CO_2^-$ O atom bridges the Ni2−Ni4 vector, and the $O^-$ group $\mu_3$-bridges Ni4, Ni5, and Ni7. The remaining carboxylate groups function as monodentate capping ligands to Ni5 ($\beta$) and Ni7 ($\alpha$). In mode 3, the $\alpha$-$CO_2^-$ group $\mu_2$-bridges Ni3 and Ni6 in a 1,1 mode. The $O^-$ group is also $\mu_2$-bridging (Ni6 and Ni8), with one $\beta$-$CO_2^-$ group monodentate capping Ni6 and the remaining $\beta$-$CO_2^-$ group 1,1,3-bridging Ni8, Ni9, and Ni11. In mode 4, the Ni4−Ni5 vector is bridged by a $\beta$-$CO_2^-$ group. The $O^-$ group $\mu_2$-bridges Ni5 and Ni8, with the $\alpha$-$CO_2^-$ group capping Ni8, and the remaining $\beta$-$CO_2^-$ group 1,1,3-bridging Ni8, Ni9, and Ni10. It is interesting to note that, in both the third and fourth modes, five nickel centers are bridged as one $\beta$-carboxylate group increases its coordination from 1,1-bridging (as in modes 1 and 2) to 1,1,3-bridging. In modes 5 and 6, three nickel centers are bridged. In both cases, the $O^-$ group and one $\beta$-$CO_2^-$ group are $\mu_2$-bridging, with the $\alpha$-$CO_2^-$ group and the second $\beta$-$CO_2^-$ group monodentate capping. Therefore, five different bonding modes are observed within the cluster.

The structure is made even more interesting by the presence of stereoisomerism. If we take a line through the center of the core (Ni2−Ni1−Ni2′) (Figures 1 and 2), compound **1** can be described as the $\Delta-\Lambda$ form, whereas compound **2** comprises a pair of enantiomers with the $\Delta-\Delta$ and $\Lambda-\Lambda$ configurations. Isomerism has been observed previously in $Mn_{12}$ complexes, but this is a geometric isomerism where the positions of $H_2O$ and carboxylate ligands differ.[35] However, in our system, the points of ligation of the citrate and $H_2O$ ligands are identical for both **1** and **2**. We are unaware of other examples of stereoisomerism in such large spin clusters, and it will be interesting to see

(30) *Gmelins Handbuch der anorganische Chemie*; VCH: Weinheim, 1966; Vol. 57 B 3; p 894.
(31) Powell A. K.; Heath, S. L.; Gatteschi, D.; Pardi, L.; Sessoli, R.; Spina, G.; Del Giallo, F.; Pieralli, F. *J. Am. Chem. Soc.* **1995**, *117*, 2491.
(32) Brechin, E. K.; Harris, S. G.; Harrison, A.; Parsons, S.; Whittaker, A. G.; Winpenny, R. E. P. *Chem. Commun.* **1997**, 653.
(33) Murray, K. S. *Adv. Inorg. Chem.* **1996**, *43*, 322.
(34) Liu, W.; Thorp, H. H. *Inorg. Chem.* **1993**, *32*, 4102.
(35) Aubin, S. M. J.; Sun, Z.; Eppley, H. J.; Rumberger, E. M.; Guzei, I. A.; Folting, K.; Gantzel, P. K.; Rheingold, A. L.; Christou, G.; Hendrickson, D. N. *Inorg. Chem.* **2001**, *40*, 2127.

whether this is a feature common to other citrate-assembled compounds.

**4.2. Magnetic Properties.** The value of $\chi T$ at room temperature in the limit of no interaction between the individual ions is theoretically given by

$$\chi T = \frac{N_A \mu_B{}^2 g^2}{3k} n S_i(S_i + 1) \quad (1)$$

with $S_i$ being the spin of one ion ($S_i = 1$ for $Ni^{2+}$) and $n$ the number of spin carriers ($n = 21$). The experimental value of 26.8 emu $mol^{-1}$ K at 300 K, see Figure 5, is consistent with 21 uncoupled $S_i = 1$ spins and a $g$ value of 2.26. The decrease of $\chi T$ with decreasing temperature is an indication of dominant antiferromagnetic interaction between the nickel ions within the cluster. At extremely low temperatures, where only the cluster ground state with spin $S$ is populated, $\chi T$ is given by

$$\chi T = \frac{N_A \mu_B{}^2 g^2}{3k} S(S + 1) \quad (2)$$

At 2 K the experimental $\chi T$ value is 9.4 emu $mol^{-1}$ K, which is between 7.7 and 12.9 emu $mol^{-1}$ K calculated for $S = 3$ and $S = 4$, respectively. This is consistent with a spin ground state of 3, but with higher spin excited states which are still populated at 2 K. This kind of situation is not unusual with such a large cluster and a large number of spin states (approximately $1 \times 10^{10}$).

To model the magnetic data, we tried to correlate the sign of the exchange interaction of neighboring nickel ions to the Ni−O−Ni angle. Previous reports showed that a bridging angle lower than 98° predominantly leads to ferromagnetic interaction.[33,36] Within the Ni−OH core many angles are close to 98°, and therefore, it is very difficult to decide whether the interaction is ferromagnetic or antiferromagnetic. Thus, we treat the core as a fragment of $Ni(OH)_2$, which shows ferromagnetic coupling within the layers.[37] We built upon that core to predict the sign of the adjacent interactions and continued like that toward the end of the molecule. Since there are competing interactions, we could not determine an exact value, but using this simple approach the ground-state spin value must lie between $S = 1$ and $S = 5$. Hence, the experimentally determined $S = 3$ ground state is very reasonable on the basis of these magnetostructural correlations.

The field dependence of the magnetization measured below 200 mK supports the conclusion of an $S = 3$ ground state (see Figure 6). At low field the magnetization increases sharply. However, saturation could not be observed at a value of $M/N_A\mu_B = 6.8$ expected for $S = 3$ and $g = 2.26$ (with $M/N_A\mu_B = gS$ at saturation), because of excited spin states with higher $M_S$ values being stabilized as the field is increased. This lowering leads to at least one spin crossover showing up as a clear step in the magnetization curve, similar to the crossovers observed in the "molecular ferric wheel".[38] At 7.5 T the magnetization reaches a value of $M/N_A\mu_B = 19.8$, indicating that excited spin states as large as $S = 9$ must lie close in energy to the ground state. The differences between the magnetization curves for different orientations of the crystal to the field are a sign of the anisotropy of the magnetic properties of the cluster.

The frequency-dependent out-of-phase signals in the ac susceptibility (Figures 8b and 9b) are clear evidence of a slow relaxation process at temperatures below 800 mK of this experiment. The ac data are not perfectly smooth, which could be due to the small mass of the single crystal used and/or temperature instability during the measurements. From the frequency dependence of the ac signal in the range 0.111−1111 Hz we conclude that the time scale of the relaxation is on the order of 1 s at 200 mK. For a quantitative analysis we correlated the frequency dependence of the ac signal to an Arrhenius law:

$$\tau = \tau_0 \exp(\Delta E/kT) \quad (3)$$

Arrhenius behavior could only be observed for measured frequencies between 21 and 1111 Hz for one orientation of the crystal (field along the $b^*$-axis) and for frequencies between 111 and 1111 Hz with the field along $c$. In the measurement parallel to the $a$-axis the high-frequency part was not measured due to problems with the sample holder. The fitting of $\ln \tau$ versus $1/T$ (see Figure 9) yielded the two parameters $\tau_0 = 1.1 \times 10^{-5}$ s and $\Delta E = 1.7$ K for the field along the $b^*$-axis and $\tau_0 = 4.0 \times 10^{-7}$ s and $\Delta E = 2.9$ K for the field along the $c$-axis.

Deriving the easy axis in such a complex molecule from ac susceptibility measurements is difficult. Furthermore, we were only able to measure the high-frequency data that allow access to $\Delta E$ along two directions. Referring back to Figure 3, the $c$-axis passes along the compact body of the cluster where $\Delta E = 2.9$ K. Perpendicular to $c$, $b^*$ lies approximately in the $\{Ni_7(OH)_6\}$ plane, where $\Delta E = 1.7$ K. Since the value of the ac susceptibility is largest with the field along the $c$-axis, we conclude that in this orientation the direction of the field is closest to the easy axis of magnetization. Alternatively, it could be argued that the easy axis would lie approximately perpendicular to the $\{Ni_7(OH)_6\}$ plane. However, we were unable to measure the high-frequency data along this direction to gain access to $\Delta E$.

We conclude that the slow relaxation originates in an energy barrier for the reversal of the direction of magnetization that arises when the spin ground state is zero-field-split with a negative $D$ parameter. Since the cluster symmetry is not axial, we have to include a rhombic term in the ZFS Hamiltonian, which is therefore given by

$$\hat{H}_{ZFS} = D[S_z{}^2 - (1/3)S(S + 1)] + E(S_x{}^2 - S_y{}^2) \quad (4)$$

The nonzero value of $E$ leads to a mixing of the wave functions originally differing by $\Delta M_S = \pm 2$ and thus enables

(36) Halcrow, M. A.; Sun, J.-S.; Huffman, J. C.; Christou, G. *Inorg. Chem.* **1995**, *34*, 4167.
(37) Rouba, S.; Rabu, P.; Ressouche, E.; Regnault, L.-P.; Drillon, M. *J. Magn. Magn. Mater.* **1996**, *163*, 365.
(38) Taft, K. L.; Delfs, C. D.; Papaefthymiou, G. C.; Foner, S.; Gatteschi, D.; Lippard, S. J. *J. Am. Chem. Soc.* **1994**, *116*, 823.

quantum tunneling. This reduces the effective height of the energy barrier to a lower value than the energy difference between the $M_S = \pm 3$ and $M_S = 0$ states. In axial symmetry this latter energy difference is given by $\Delta = S^2|D|$. If the symmetry were purely axial in $Ni_{21}$, we could equate $\Delta E$ found by ac susceptibility measurements with $\Delta$. This would give a $D$ value of $-0.32$ K (along $c$). The $D$ value obtained in this way is approximately half the $D$ of dodecamanganese acetate.[39] We must bear in mind, however, that our cluster is not axial. As a result of the $E$ term in eq 4, tunneling contributes to the relaxation, and the $D$ value determined above is a lower limit of the actual anisotropy parameter. In the presence of small transverse anisotropy the relaxation short-circuits the top of the barrier by thermally activated tunneling. In this case the relaxation still follows an Arrhenius law,[40] but $\Delta E$ is smaller than the real barrier $\Delta$. In the presence of a stronger transverse anisotropy, tunneling processes are even more favored and can occur between lower lying $M_S$ levels, and the wave functions near the top of the barrier are strongly admixed. Thus, $M_S$ is no longer a good quantum number, and the barrier height cannot be calculated as $S^2|D|$. The high-temperature part of the ac susceptibility along the $c$-axis accounts for the thermally activated relaxation of the magnetization, as it could be fit to an Arrhenius law, see Figure 9b, whereas below 300 mK the relaxation is mainly caused by tunneling processes. A similar behavior was found in the SMM $Fe_8$, which follows an Arrhenius law down to 350 mK, before the relaxation becomes completely temperature independent due to quantum tunneling of the magnetization between $M_S = \pm 10$ states.[40,41] The relaxation in the $Ni_{21}$ cluster does not show a total independence of the temperature, but at lower temperatures the relaxation clearly becomes faster than expected for a thermal process. In the measurements with the field perpendicular to the $c$-axis, the transverse part of the magnetic field is clearly larger and tunneling processes are more favored. Therefore, the $\Delta E$ value found with the field parallel to the $b^*$-axis could reflect an activation energy which is much lower than the energy barrier and also lower than the $\Delta E$ value found from the measurements along the $c$-axis.

## 5. Conclusions

In the present study we have shown that it is possible to build high-nuclearity clusters using the polydentate ligand citrate, and that the $Ni_{21}$ clusters we obtained exhibit a remarkable stability. We could determine the spin ground state of the cluster, although things are rather complicated due to close-lying excited states with a higher spin multiplicity. Measurements in the millikelvin temperature range clearly show the typical slow magnetic relaxation behavior of single-molecule magnets. We could also obtain an estimate of the axial ZFS parameter through the height of the energy barrier. The barrier is not very high because of the small ground-state spin, but clearly SMM behavior could be observed due to the magnetic anisotropy. This study certainly highlights the potential for creating new single-molecule magnets using $Ni^{2+}$.

**Acknowledgment.** The financial support of the Swiss National Science Foundation (NRP47 "Supramolecular Functional Materials") and the European Community (Fifth Framework Programme MOLNANOMAG HPRN-CT-1999-00012) is gratefully acknowledged. S.T.O. thanks C. Paulsen and E. N. Khatsko from the CRTBT—CNRS for hospitality and support.

**Supporting Information Available:** Crystallographic files for **1** and **2** in CIF format. This material is available free of charge via the Internet at http://pubs.acs.org.

IC020252W

(39) Caneschi, A.; Gatteschi, D.; Sangregorio, C.; Sessoli, R.; Sorace, L.; Cornia, A.; Novak, M. A.; Paulsen, C.; Wernsdorfer, W. *J. Magn. Magn. Mater.* **1999**, *200*, 182.
(40) Barbara, B.; Thomas, L.; Lionti, F.; Chiorescu, I.; Sulpice, A. *J. Magn. Magn. Mater.* **1999**, *200*, 167.
(41) Wernsdorfer, W.; Sessoli, R. *Science* **1999**, *284*, 133.